3 Ring-Ring Design

J. Beebe-Wang, J.S. Berg, M. Blaskiewicz, J.M. Brennan, A. Fedotov, W. Fischer, H. Hahn, Y. Luo, C. Montag, R. Palmer, S. Peggs, V. Ptitsyn, K. Smith, S. Tepikian

3.1 Ring-Ring Design Concept

The ring-ring design provides an alternative path towards a machine design with a nominal luminosity in the $10^{33}cm^{-2}sec^{-1}$ regime, upgradable to$10^{34}cm^{-2}sec^{-1}$ by conversion to a linac-ring scheme, as covered in Chapter 1. The nominal ring-ring design described here uses existing technologies almost exclusively, thus greatly reducing the technical risk of the design. This results in less required budget contingency, which reduces project cost, and a fast commissioning process, thus providing useable physics data after a short amount of time.

The basic assumptions of this design are:

1. The electron ring is installed in the existing RHIC tunnel to minimize costly civil engineering.
2. There is only one interaction region, with one detector. Luminosities and beam-beam parameters quoted are based on a single beam-beam interaction per turn. This does not preclude later operations with two detectors, with the associated effect on luminosity.
3. Electron and hadron beams have identical beam sizes at the interaction point, with the horizontal beam size being larger than the vertical. At the interaction point the two beams intersect at a full crossing angle of 15 mrad in the horizontal plane. The resulting luminosity loss will be largely restored by crab cavities in the hadron beamline. Crab cavities in the electron ring are an option, but are not considered necessary at this point due to the much shorter electron bunch length.
4. Hadron beam parameters are a moderate extrapolation of what has been achieved at RHIC, with the exception of the number of bunches which will be increased 3-fold, from 120 to 360.
5. A recirculating linac inside the RHIC tunnel serves as full-energy injector of polarized beam for the electron storage ring. This injector can later be converted to an Energy Recovery Linac colliding directly with the stored hadron beam in a linac-ring scheme.
6. The maximum electron beam-beam parameter does not exceed 0.1, a level that has been routinely achieved at the B-factories KEKB and PEP-II even with synchrotron radiation damping decrements that are ten times smaller than in eRHIC. The electron ring will be operated near the half-integer betatron resonance to minimize the beam-beam effect.
7. The RF power installed in the electron storage ring is 10 MW, corresponding to a linear synchrotron radiation power load of 4 kW/m in the arcs.

To reduce overall cost, reusing components of the existing, decommissioned PEP-II storage rings at SLAC is planned. This includes all necessary quadrupole and sextupole magnets as well as all dipole correctors needed for the eRHIC electron storage ring, resulting in significant cost savings. This electron storage ring will be installed above the existing RHIC rings to minimize interference with the hadron ring. This is accomplished by sets of dipole magnets in the hadron ring, forming

vertical dog legs between the low-β doublets and the arcs. Additional dipole magnets serve to separate the hadron beam from the 4 mrad neutron cone that needs to be detected outside the central detector.

3.2 Beam Parameter and Luminosities

The nominal ring-ring scenario assumes hadron beam parameters similar to those already achieved in RHIC, with some modest extrapolations. For instance, proton bunch intensities of up to 3×10^{11} protons per bunch are assumed in the design, a 25% increase over the 2.4×10^{11} routinely achieved in RHIC Run-15. The existing 28 MHz RF system can store the 360 bunches assumed in this design, although an injection kicker with a faster rise time is required. Resistive wall losses and the associated heating of the cold beam pipes are issues, as is the heating of the Beam Position Monitor (BPM) cables. Beam pipe heating can be overcome to some extent by providing more cooling power from the existing RHIC cryogenic plant while BPM cables inside the cryostats need to be replaced.

The normalized RMS transverse proton beam emittance of 2.5 μm is identical to what is routinely achieved in RHIC. An RMS bunch length of 20 cm is achievable with 250 GeV proton beams with current beam parameters; at lower energies longitudinal electron cooling is required to limit the momentum spread.

Since no transverse cooling of the proton beam is assumed, RMS proton beam sizes at the interaction point (IP) vary with the proton beam energy. The aperture of the focusing elements in the hadron ring is chosen such that proton β-functions at the IP can be kept constant over the entire proton beam energy range from 50 to 250 GeV. The apertures of the focusing elements in the electron ring are designed such that they can accommodate an electron beam that collides with 250 GeV protons presenting the smallest occurring beam size at the IP, with the RMS electron beam emittances being 53 nm horizontally and 9.5 nm vertically.

When the proton beam energy is lowered, the proton beam sizes at the IP increase due to the increasing emittance at constant β as

$$\sigma^2(E) = \epsilon_e(E)\beta_e(E) = \sigma^2(250\ GeV)\frac{250}{E(GeV)}$$

To accommodate the electron beam in the low-β focusing elements the angular divergence of the electron beam must be kept constant,

$$\sigma'^2 = \frac{\epsilon_e(250G\ eV)}{\beta_e(250\ GeV)} = \frac{\epsilon_e(E)}{\beta_e(E)} = k$$

Combining these two equations yields

$$\beta_e^2 = \frac{250}{kE(GeV)}\sigma^2(250\ GeV)$$

A corresponding scaling rule for the electron emittances can be derived in a similar fashion.

Based on these parameters, the bunch intensities of both beams can then be calculated by limiting the beam-beam parameters to 0.015 for the proton beam and 0.1 for the electron beam while simultaneously limiting the synchrotron radiation losses at any given electron energy to 10 MW, and capping the proton bunch intensity at 3×10^{11}. The resulting luminosity curves for different proton beam energies are depicted in Figure 3-1; some key beam parameters are listed in Table 3-1.

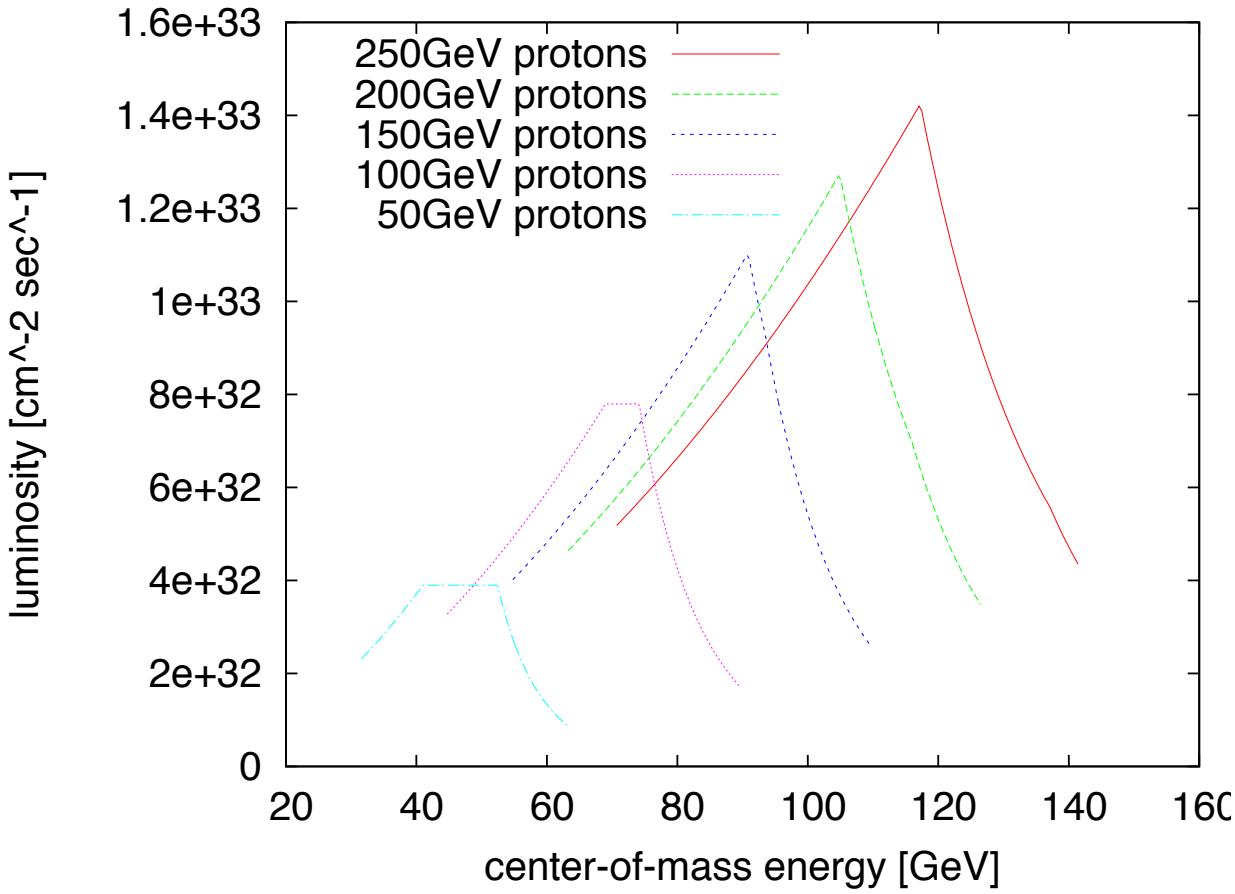

Figure 3-1: The resulting luminosity curves for different proton beam energies.

Table 3-1: Electron-proton parameters for highest luminosity.

	Electrons	Protons
Energy [GeV]	13.7	250
Bunch intensity	$2.1\text{x}10^{11}$	$2.1\text{x}10^{11}$
Beam current [mA]	935	935
Emittance h/v [nm]	53/9.5	9.5/9.5
Beta h/v [m]	0.38/0.27	2.16/0.27
Beam-beam parameter	0.1	0.015
RMS bunch length [cm]	1	20
polarization [%]	80	70
peak luminosity [$\text{cm}^{-2}\text{sec}^{-1}$]	$1.41\text{x}10^{33}$	

The electron cooler required for longitudinal cooling of proton beams at lower energies will be utilized for the reduction of gold beam emittances at all energies. Transverse RMS gold beam emittances of 9.5 nm, and RMS bunch lengths of 20 cm are assumed regardless of beam energy. As a consequence, electron emittances are also constant at 53 nm horizontal and 9.5 nm vertical, as are the ion and electron β-functions. As in the proton case, maximum bunch intensities are calculated

based on the allowable beam-beam parameters and the total synchrotron radiation losses, while the gold ion bunch intensity is capped at 2.0×10^{9}. Figure 3-2 shows the resulting luminosity curves for different gold beam energies; the corresponding beam parameters are listed in Table 3-2.

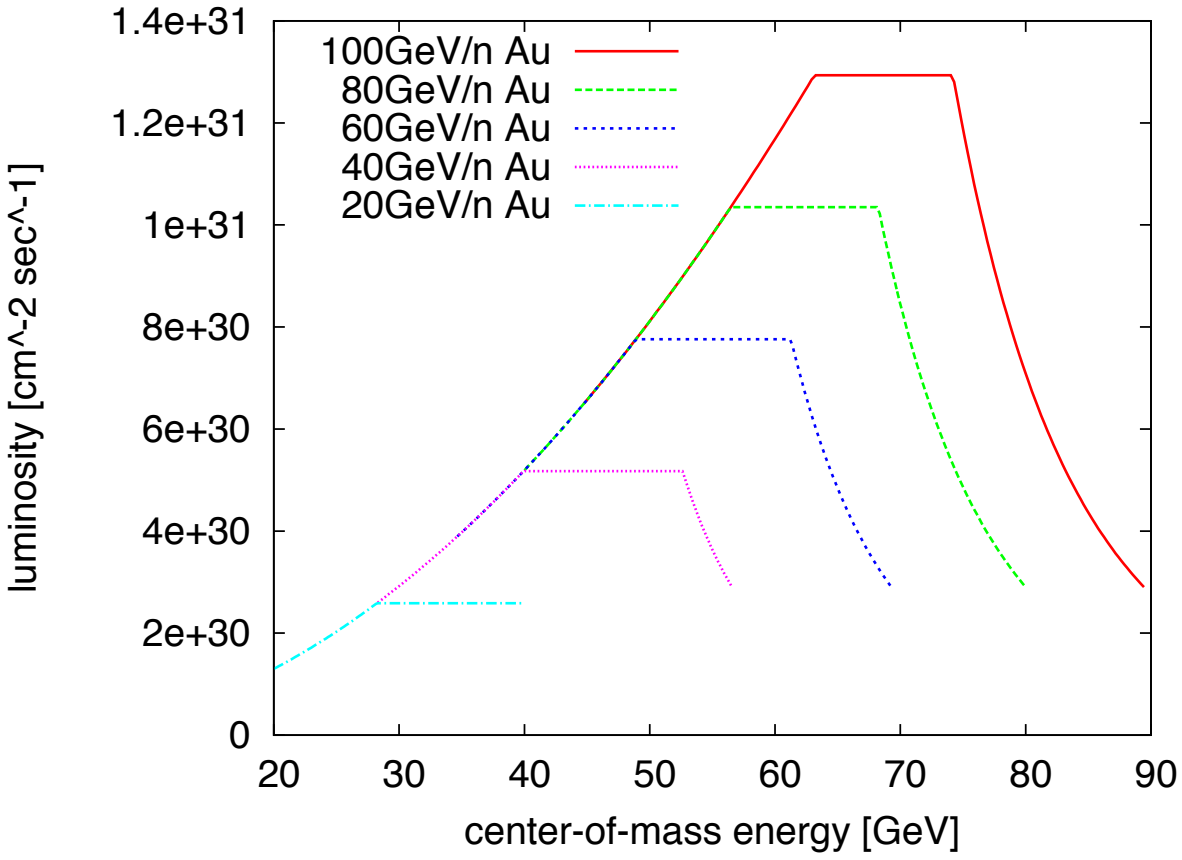

Figure 3-2: The resulting luminosity curves for different gold beam energies.

Table 3-2: Electron-gold parameters for highest luminosity.

	Electrons	Au ions
Energy [GeV]	13.7	100
Bunch intensity	$2.1\text{x}10^{11}$	$2.0\text{x}10^{9}$
Beam current [mA]	935	712
Emittance h/v [nm]	53/9.5	9.5/9.5
Beta h/v [m]	0.38/0.27	2.16/0.27
Beam-beam parameter	0.073	0.015
RMS bunch length [cm]	1	20
polarization [%]	80	
peak luminosity [$\text{cm}^{-2}\text{sec}^{-1}$]	$1.28\text{x}10^{31}$	
peak luminosity/nucleon [$\text{cm}^{-2}\text{sec}^{-1}$]	$2.52\text{x}10^{33}$	

3.3 Lattice and Optics

3.3.1 Modifications to RHIC

RHIC Injection Kickers

The 28 MHz bunching frequency necessitates new injection kickers in RHIC. Take a full bunch length of $T_b = 15$ ns, a bunch spacing of $T_s = 35$ ns. We assume a strip line kicker of length $L = 1.25$ m. If we assume the kicker pulse starts just as the previous bunch passes and hits its peak just before the injected bunch then the rise time satisfies:

$$T_r \le T_s - T_b - 2L/c = 12\ ns$$

We take a rise time of 10 ns which has been achieved in practice. A flattop voltage of 30 kV is reasonable. We take a deflection angle of 0.002 rad, as is now the case. If we take a stripline kicker of characteristic impedance 50 Ω and a horizontal plate spacing of 5 cm then the current in each plate will be 600 A. For a 24 GeV proton beam we need a total of 16 such modules. The active length of 19.2 m does not include bellows, pumping ports etc, so a total length of 25 m is taken for the injection kicker. The present injection area in the RHIC tunnel does not allow for a 25 m kicker. It will be necessary to shift the cryostat containing Q4 through Q7 closer to the triplet in IR6. The broken symmetry may not allow this to remain an experimental IR. However, a shift of the same size on the other side of the IR might be compatible with an experiment.

3.3.2 Electron Ring Lattice

The electron storage ring properties presented here are defined by the baseline parameters given in the Table 3-3. In this table, the configurations of "Low", "Middle" and "High" energy correspond to collisions with 50, 130 and 250 GeV protons, respectively. The FODO cell was chosen to achieve the high packing factor necessary to reduce the electron power needed for operation. The emittance requirements are achievable with the FODO cell with dimensions shown in Figure 3-3.

Table 3-3: Some of the design goals for the electron storage ring in the baseline Ring-Ring eRHIC.

Energy configuration	Low	Middle	High
Energy [GeV]	5	20	20
Beam current [A]	0.925	0.508	0.508
U_0 [MeV]	0.18	47.1	47.1
ε_x , ε_y [nm]	106.0, 19.0	62.2, 11.2	53.0, 9.5
β_x^* , β_y^* at IP [m]	0.86, 0.60	0.61, 0.42	0.38, 0.27

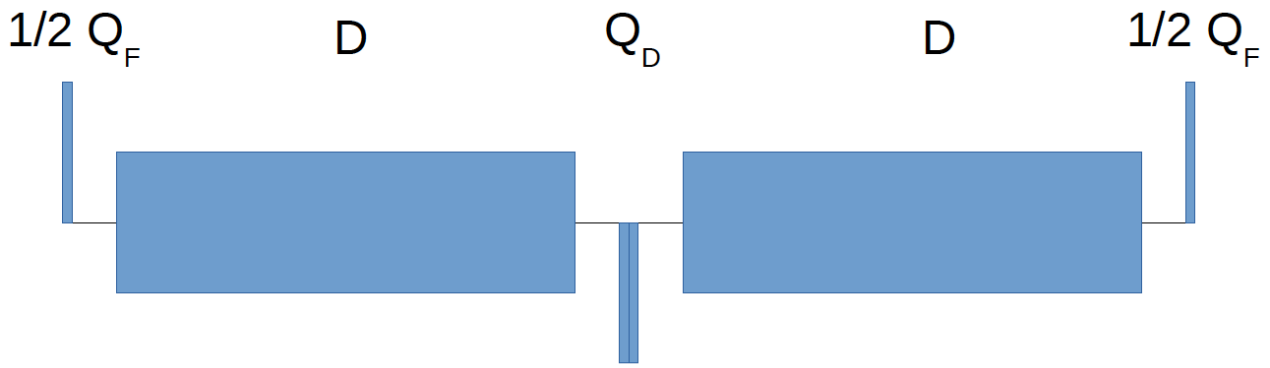

Figure 3-3: The FODO cell used where L_Q = 0.4 m (quadrupole length), L_S = 1.0 m (drift space length) and L_D = 10.123825 m (dipole length). The 1.0 m drift space between magnets is used to provide enough space for sextupoles, orbit corrector, BPMs etc.

The ring is designed using a modular approach with (1) FODO cells in the arcs followed by, (2) dispersion suppressor at each arc end, (3) two colliding IRs which could be tuned to a high β^* for non-colliding mode, (4) three dispersion free straight sections and (5) a special straight section with dispersion where the Robinson Wiggler [1] is placed, to achieve the required emittance in the low energy configuration. The IRs and straight sections use a symmetric optics. Large drift spaces are available for additional devices such as RF cavities, additional sextupoles, spin rotators, etc. Figures 3-4, 3-5 and 3-6 show the full ring optics for the three different energy configurations: high, middle and low respectively.

The dispersion suppressor is designed for a 60° cell. Using a lower phase advance would require negative bends in the dispersion suppressor. Using six quadrupoles, the dispersion suppressor can be optimized for different cell phase advances. Except for low energy with a cell phase advance near 60°, the cell phase advance is near 90° as shown in Table 3-4.

There are four ways to change the emittance in an electron ring: (1) select the type of cell: FODO, DBA, TBA, TAL, etc. (2) change the cell length, (3) change the phase advance of the cell and (4) add wigglers. Table 3-4 shows the relationship between cell length and phase advance for the FODO cell on the emittance. The FODO cell shown in Figure 3-3 was selected. Note the arc length used in Table 3-4 is not the arc length of the final ring. The final ring used 18 cells per arc – including the dispersion suppressors – with an arc length of 450.858 m. The arc length was determined such that the electron beam collides at the existing RHIC collision points and with a trajectory circumference of 3833.845 m. At low energy, to achieve the design emittance, it was also necessary to add a wiggler.

Table 3-4: Given an arc of length 445.066 m and a total bending angle 60°, this table shows the cell phase advance needed to get to an emittance of 53 nm at different energies. Figure 3-3 shows the need for 2.4 m of drift spaces and quadrupoles. Column: #1 is the number of cells per arc, #2 is the cell length, #3 is the dipole length, #4 shows the dipole bending radius, #5 is the packing factor and #6-9 show the cell phase advances needed to get 53nm at energies 5, 10, 15 and 20 GeV, respectively.

		FODO Cell						
					Beam energy [GeV] at 53 nm			
N_{cells}	L_{cell} [m]	L_D [m]	ρ [m]	PF [%]	5	10	15	20
16	27.8166	11.5083	307.7095	72.4011	41.6609	66.7309	89.2446	113.0798
17	26.1803	10.6902	306.2509	72.0579	39.0228	62.3768	83.0294	103.6440
18	24.7259	9.9629	304.4450	71.6330	36.7232	58.6099	77.7638	96.2944
19	23.4245	9.3123	302.3468	71.1393	34.7012	55.3159	73.2226	90.2180
20	22.2533	8.7266	300.0000	70.5871	32.9096	52.4095	69.2544	85.0392
21	21.1936	8.1968	297.4402	69.9848	31.3115	49.8256	65.7512	80.5409

The Robinson Wiggler consists of four dipole magnets with a non-zero gradient, as seen in Figure 3-7. This wiggler inside a dispersion straight section will change the damping partition number. A significant change of up to 3 damping partition units is achievable. Without this wiggler the emittance for the low energy configuration is about 10nm with a 60° cell phase advance (which gives about a factor of 3 over the 90° cell). Thus, the wiggler required to increases the horizontal emittance by a factor of 10. Note, for positive dispersion, the wiggler decreases horizontal emittance, while with negative dispersion, the wiggler increases horizontal emittance.

There are 314 quadrupoles in this lattice. Most of the quadrupole lengths are the same as the arc quadrupole lengths. Some of the quadrupoles in the IR regions needed to be longer. There are 192 dipoles in the arcs, all of the same length whose properties are shown in Table 3-5. Four additional dipoles with gradients are needed for the Robinson Wiggler.

Finally, Table 3-5 list some of the properties calculated using MADX [2]. In this table, the configurations of “Low”, “Middle” and “High” energy correspond to collisions with 50, 130 and 250 GeV protons, respectively.

There is enough flexibility in the design to use the longer PEP-II [3] quadrupoles. There are many questions that need to be asked such as: can these magnets with their existing cooling systems be worked into this ring.

Table 3-5: This table shows the parameters for the ring in the three energy configurations of the baseline design. The "Design Tunes", "Cell Phase Adv" and "Natural chromaticity " rows give the "horizontal, vertical" values. The "Horizontal chromaticity" and "Vertical chromaticity" rows show the "1st order, 2nd order, 3rd order" chromaticity values from PTC in MADX with two families of sextupoles in the cells. The row "α_{xx}, α_{xy} (or α_{yx}), α_{yy}" gives the amplitude dependent tune effects due to the sextupoles. The "High" energy configuration has very strong chromatic effects which can be reduced by setting the vertical tune to 39.18 (below the horizontal tune).

4 Energy Configuration	Low	Middle	High
Energy [GeV]	5	20	20
Design tunes	28.72, 29.82	38.28, 39.18	40.28, 41.18
Cell phase Advance [degree]	61.76, 65.23	88.06, 91.37	95.07, 111.82
Cell length [m]	25.0476505		
Dipole length [m]	10.12382525		
ρ [m]	309.3613117		
Circumference [m]	3833.845181		
Momentum compaction	0.00231	0.00123	0.00110
Natural chromaticity	-45.375, -43.148	-66.414, -67.209	-80.293, -76.710
Horizontal chromaticity	1.83, 140.4, 46738	1.86, 359.5, 83866	1.85, 725.9, 673201
Vertical chromaticity	1.88, 129.9, 26794	1.90, 186.6, 11078	1.88, -2030.2, 884622
α_{xx}, α_{xy} (or α_{yx}), α_{yy}	-272.3, -850.5, -165.3	37.35, -2315, 32.52	4661, 3748, 3348
β_{max} [m]	269.1	379.4	603.8
Horizontal emittance ε [nm]	109.3	62.52	52.37
J_x	0.0994339	0.99509099	0.99512338
J_E	2.90063429	2.00490632	2.00487382
U_0 [MeV/turn]	0.187	45.755	45.754
Beam current [A]	0.925	0.508	0.508
Total SR power [MW]	0.173	23.243	23.243

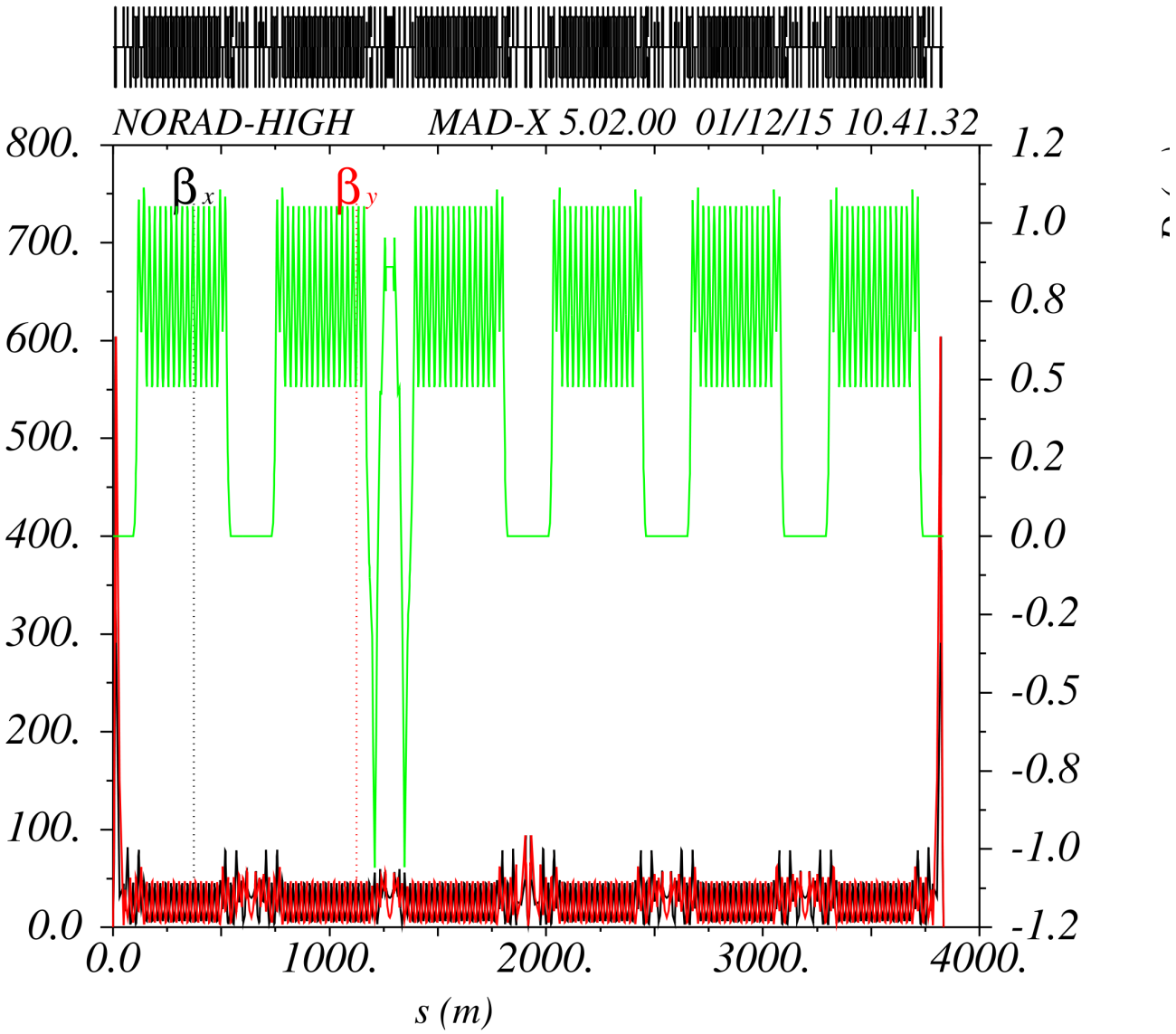

Figure 3-4: Full electron ring for the "High" energy configuration (collision with 250 GeV protons).

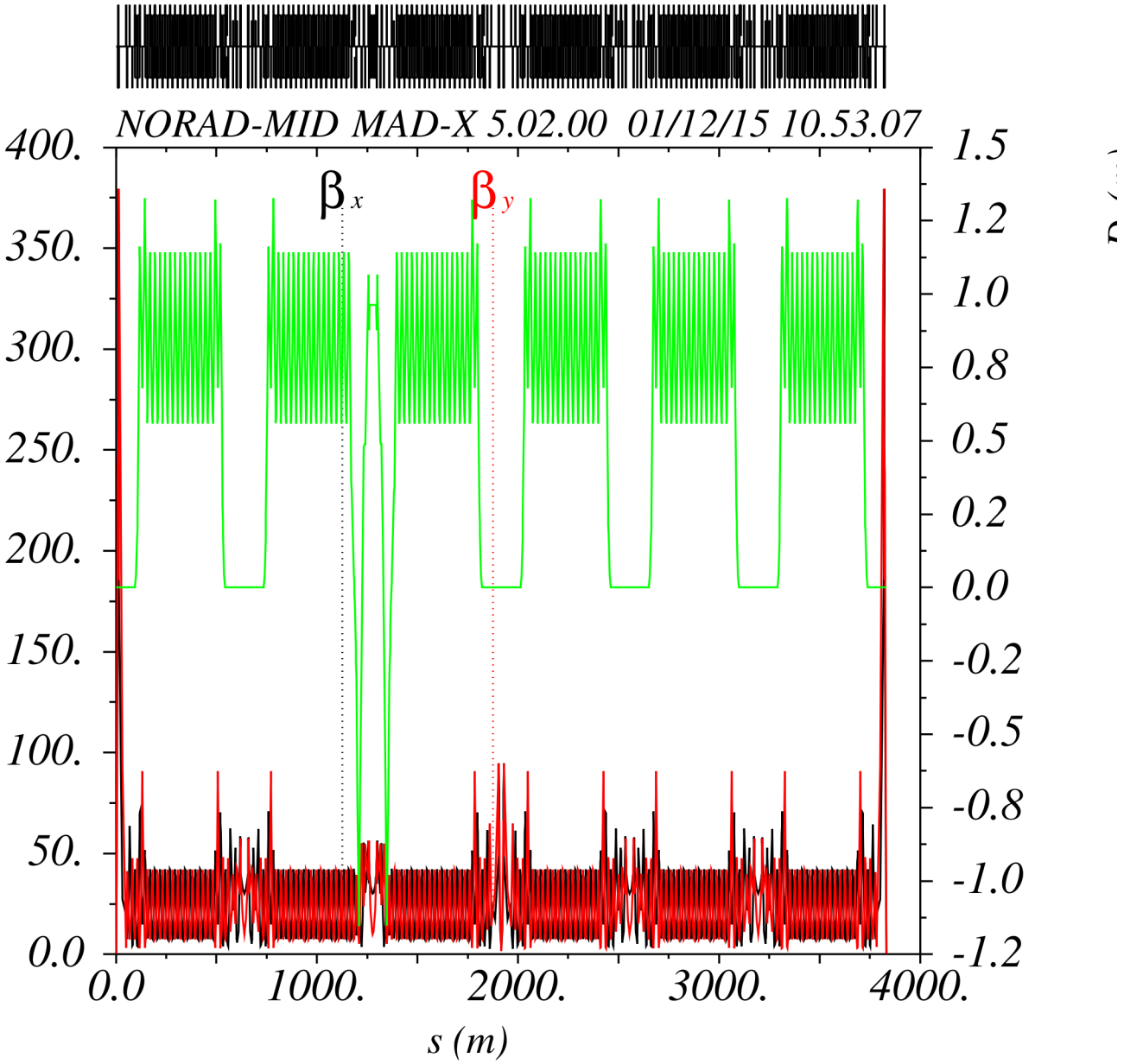

Figure 3-5: Full electron ring for the "Middle" energy configuration (collision with 130 GeV protons).

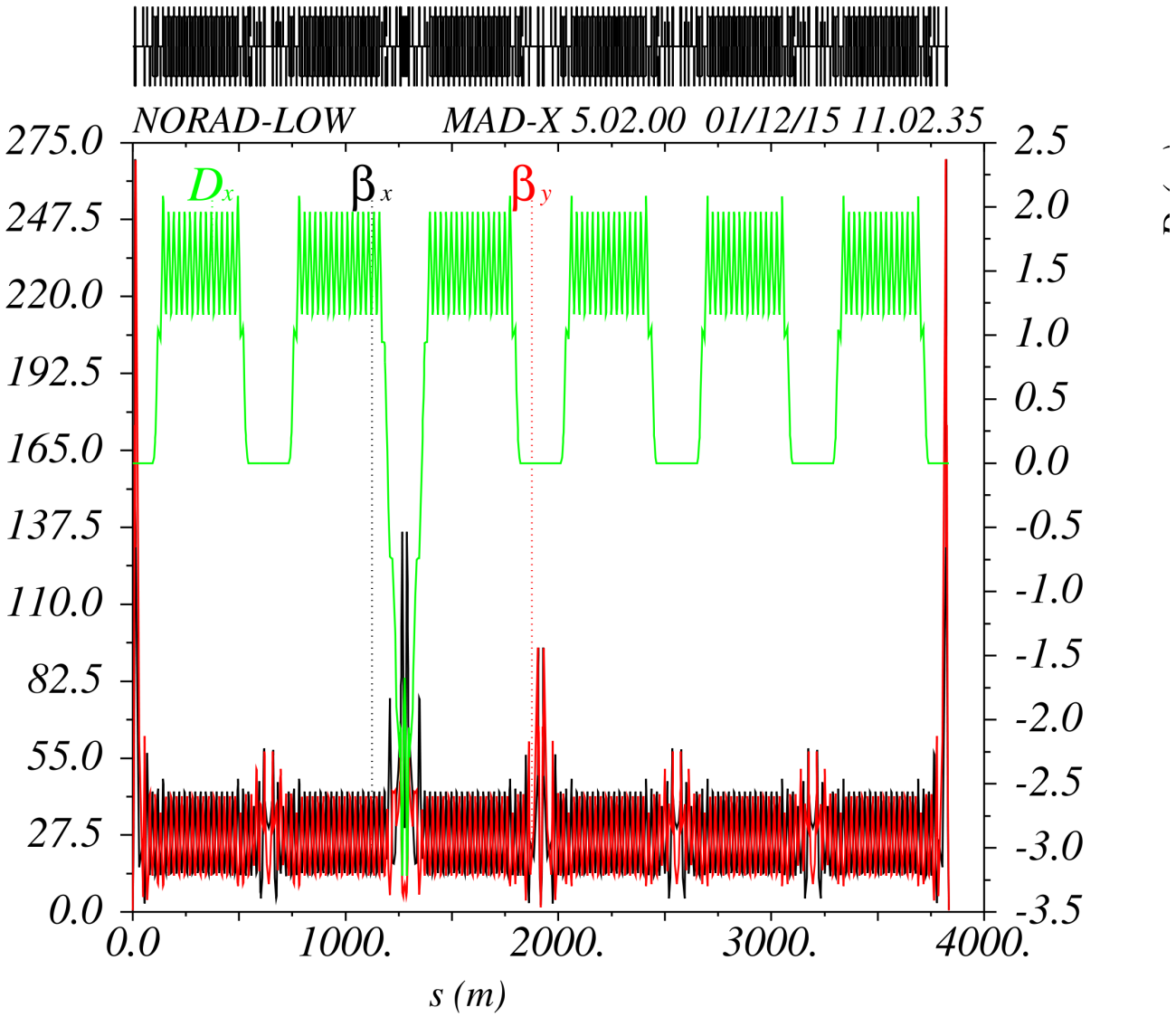

Figure 3-6: Full electron ring for the "Low" energy configuration (collision with 50 GeV protons). For the low energy, the Robinson Wiggler is used to increase the horizontal emittance.

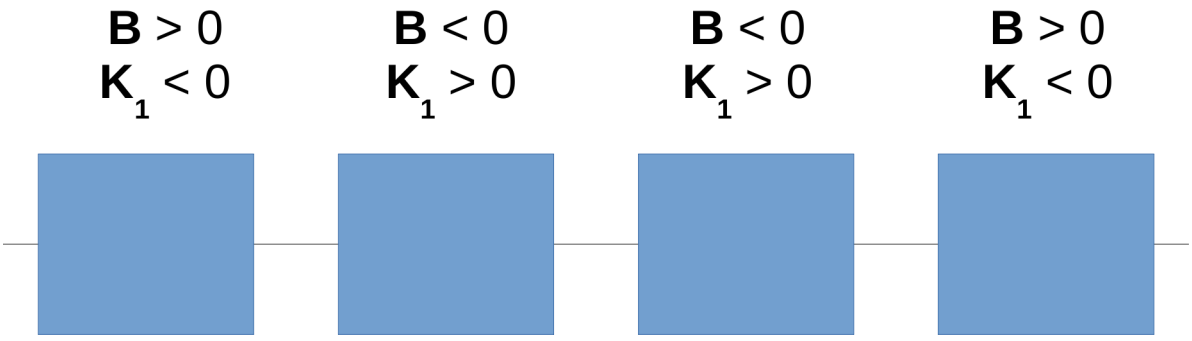

Figure 3-7: Robinson Wiggler which consists of four dipoles with gradients arranged to not change the beams closed orbit. The dipole parameters selected for the low energy configuration are length L = 7 m, dipole bending radius ρ = 170.0 m and $K1$ = 0.0235 m^{-2}.

4.1.1 Interaction Region Design

The nominal interaction region layout shown in Figure 3-8 provides ±4.5 m of free space around the interaction point for the central detector, and several meters of free space for the installation of Roman Pots between the dipoles of the horizontal dogleg in the outgoing hadron beamline (blue). In particular, Figure 3-8 illustrates four of the five angles vital in this interaction region design with their nominal (or typical) values:

- The ±4 mrad neutron cone angle is shown in green. The region within this angle of the hadron direction at the interaction point must remain free of any accelerator components to allow unobstructed detection of neutrons. To avoid background from charged particles in the neutron detector the hadron beam - and any other charged particles – is separated from the neutron cone by means of a magnetic dipole field. This field is provided by two superconducting dipole magnets with a total length of 8 m.
- The 15 mrad horizontal crossing angle between the electron (red) and the proton (blue) directions separates the beams into their respective optical channels and suppresses long-range beam-beam interactions. The luminosity loss associated with this crossing angle is largely restored by crab cavities (not shown in Figure 3-8).
- The RMS electron and hadron beam divergence angles may both be different in the two planes, depending of the beam emittances and the Twiss parameters at the interaction point. These angles determine the required apertures in the low-β magnets and associated beam pipes, with the minimum apertures being 10 σ for the hadron beam and 15 σ for the electron beam. Figure 3-8 shows the layout based on these aperture requirements.
- The proton transverse momentum acceptance angle corresponds to the minimum deflection angle that should be detectable by the Roman Pots. Such a deflected proton needs to be well outside the circulating beam, a condition that is satisfied if this deflection angle is about 10 times larger than the proton divergence angle at the interaction point. To detect protons with a transverse momentum as low as 200 MeV/c, which corresponds to a deflection angle of 0.8mrad, the beam divergence angle should therefore not exceed some 80 μrad in either plane.

Focusing of both electron and hadron beams is provided by superconducting magnets. The low-β electron triplet is located 10.2 m from the interaction point. The resulting drift space between the triplet and the central detector allows for efficient collimation of the synchrotron radiation emanating from the triplet quadrupoles. The remaining narrowed photon fan then passes safely through the central detector into the downstream electron beamline where it grazes the inner wall of the vacuum pipe further downstream. Synchrotron radiation masks in the downstream electron beamline further minimize the amount of backscattered photons entering the central detector. At the location of the electron triplet there is sufficient separation between the 15 σ electron beam and the 4mrad neutron cone for the magnet coils and steel, thus requiring only relatively small magnet apertures. Table 3-6 lists the design parameters of the individual quadrupoles in the electron low-beta triplet.

The hadron low-β doublet is located at 32m from the interaction point. Crab cavities are installed at the two ends of the horizontally focusing quadrupole QP2 where β-functions are largest. The magnet apertures as based on a 10 σ 50 GeV proton beam – where the beam size in the absence of cooling is largest – and the corresponding pole tip fields at 250 GeV are listed in Table 3-6. Separation of the hadron beam from the neutron cone is provided by a set of dipoles forming a dog leg upstream of the low-β doublet. The innermost dipole consists of two individual magnets of 4 m and 2 m length, respectively, the first one of which is tilted in the horizontal plane to maximize the distance between the coils and the electron beam. The electron beam passes just outside the cold mass of these dipoles; the magnetic field in this region is reduced to a few Gauss by means of additional coils. The long drift space between the two bends of the dogleg allows installation of Roman Pots for the detection of protons with a transverse momentum as low as 200 MeV/c.

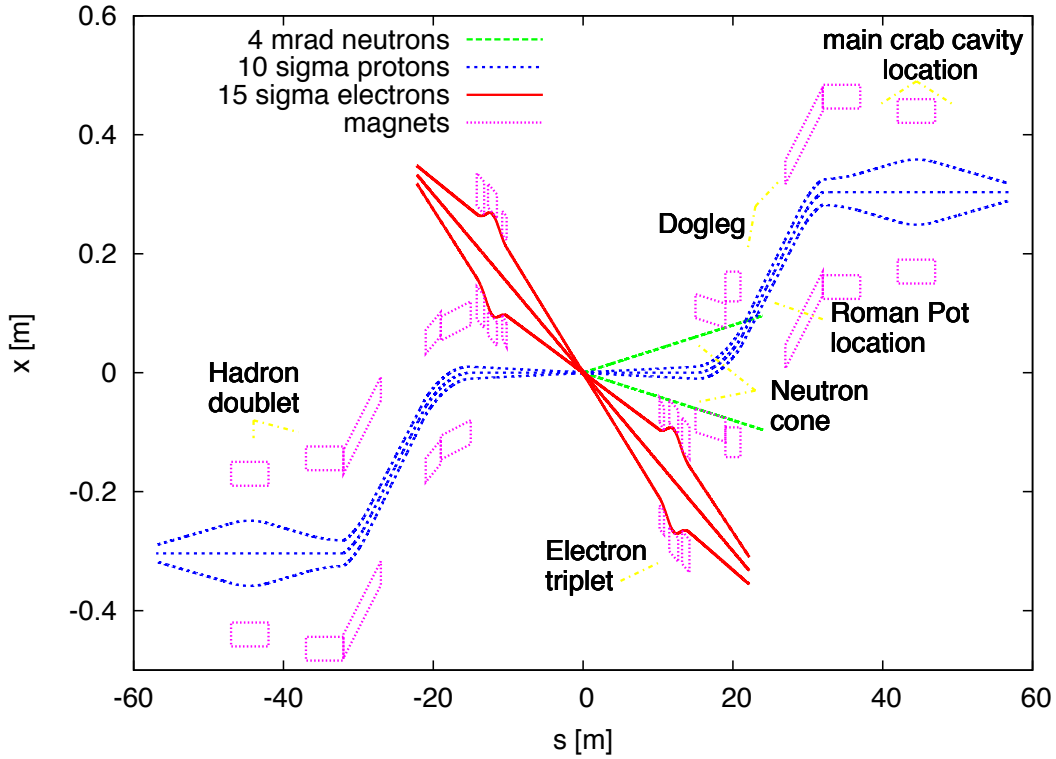

Figure 3-8: The nominal interaction region layout. Proton beam envelopes correspond to an energy of 250 GeV.

Table 3-6: Parameters of magnets.

Quadrupole	Length [m]	Strength [m^{-2}]	Aperture radius [mm]	Peak field [T]
Electron triplet				
QE1	0.6	-0.43	70	2.1
QE2	1.2	0.43	87.5	2.5
QE3	1.0	-0.30	68	1.4
Hadron doublet				
QP1	5.0	-0.022	140	2.6
QP2	5.0	0.026	115	2.6

4.2 Electron Beam Injection

The eRHIC Physics program requires highly polarized electron beams with arbitrary spin patterns. These can only be achieved by injecting full energy polarized bunches into the electron storage ring. The injector complex therefore has to be designed such that polarization is preserved during the acceleration process. This can be accomplished by a recirculating linac. While other, probably lower cost injector options do exist as well, these cannot readily be converted to a linac-ring scheme at a later time when the associated higher luminosity of such a scheme is required for an evolved Physics program. The higher initial investment into a recirculating linac injector is therefore justified by the later cost savings.

4.2.1 Recirculating Linac as Electron Injector

The entire electron injector complex is practically identical to the ERL in the linac ring scheme, as described in Chapter 2. Full intensity bunches will be generated in a SLC-type polarized gun and accelerated at a rate of 1Hz. At this low repetition rate the average beam power is negligible, making energy recovery unnecessary and reducing the HOM power in the linac to benign levels.

4.2.2 Injection Kickers and Septa

The requirement of arbitrary spin patterns in the electron ring coupled with radiative polarization necessitate regular bunch replacement. We plan to replace electron bunches every 5 minutes. With 360 bunches this corresponds to 0.8 sec between injections. The kicker will both inject the new bunch and extract the old one. There will be an injection septum on the upstream end and an extraction septum downstream. We envision several stripline kickers, which are independently powered and timed. Take a full bunch length of $T_b = 2$ ns, a bunch spacing of $T_s = 35$ ns. We assume a strip line kicker of length $L = 1.67$ m. The minimum rise and fall times satisfy:

$$T_r = T_f \le T_s - T_b - 2L/c = 23\,ns$$

We take a rise time of 10 ns and a fall time of 20 ns, which has been achieved in practice. A flattop voltage of 20 kV is reasonable. If we take a stripline kicker of characteristic impedance 50Ω and a horizontal plate spacing of 6cm then the current in each plate will be 300 A. Each plate will

bend a 20 GeV beam by 0.111 mrad. Including things like pumping ports will reduce the effective kick per meter by about 20% so we take an effective kicker strength of $k' = 5.55\times10^5$ m.

The vertical RMS emittance of the electrons in the storage ring is not more than $\varepsilon = 20$ nm and we assume the injector will satisfy this as well. Take the full length of the kicker section to be L and optimize the beta functions so that L is the value of the beta function at each end of the kicker. The stored beam size at the end will be

$$\sigma(x) = \sqrt{\varepsilon L}$$

and the RMS angular width of the stored beam will be

$$\sigma(x') = \sqrt{2\varepsilon / L}$$

To separate the beams we want the kick angle to satisfy

$$\theta_k = M\sigma(x') = M\sqrt{2\varepsilon / L}$$

with M about 10. Now the kick angle is

$$\theta_k = Lk'$$

Setting the two expressions for θ_k equal to each other with $M = 10$ gives $L = 8.65$ m and $\theta_k = 0.484$ mrad. So, we need five kicker modules and the full length of the kicker section will be about $5\times1.666\times1.2 \approx 10$ m.

Assuming a 10 m drift for the optics in the kicker region the ideal vertical beta function at the center will be 5 m and the beta function at the ends of the kicker will be 10 m. This corresponds to an RMS vertical beam size of 0.44 mm at the ends of the kicker. The vertical offset between the injected and stored beams will be $\Delta y = \frac{L\theta_k}{2} = 4.4$ mm. With a 6 cm full aperture and ± 3 cm clearance for the stored beam this leaves more than ± 2 cm for the injected beam. The stored beam has a 68 σ aperture.

4.3 RF Systems

4.3.1 Electron Ring RF

For 20 GeV electrons the synchronous voltage is 46 MeV per turn. The system is designed to handle 10 MW of synchrotron radiation. Each of the superconducting cavities used in KEKB can provide 2 MV of voltage and supply 380 kW of power to the beam. The frequency is 509 MHz. If we take a synchronous phase of 63 degrees then the total required voltage is 52 MV, which could barely be supplied by 26 cavities. If we assume 30 cavities we will have 60 MV per turn and be able to compensate 11.4 MW of synchrotron radiation power. For our application we will set the RF frequency to 18 times the $h = 360$ frequency in RHIC. This corresponds to a frequency very near 507 MHz so cavity modifications will be minimal.

The effect of beam loading is significant. The cavities have a circuit $R/Q = 50\ \Omega$ and a resonant frequency of 508 MHz. The cavity detuning is given by:

$$\delta f = -\frac{I_{RF} f_{RF}}{2V_c}\left(\frac{R}{Q}\right)\cos\phi_s$$

Where V_c is the cavity voltage, f_{RF} is the RF frequency, $I_{RF} \approx 2eN_b f_{RF}$ is the RF component of the beam current with N_b the number of particles per bunch. For $3\text{x}10^{11}$ electrons per bunch we get $I_{RF} = 2.7$ A. With $\varphi_s = 0$ and $V_c = 2$ MV we get $\delta f = 33$ kHz. This is a significant fraction of the 78 kHz revolution frequency so the complicated feedback filtering used in the B factories might be needed. The basic principles of the feedback are straightforward, employing a notch filter at the offending revolution line.

While the large voltage is necessary for operation at 20 GeV it is also helpful at lower energies to help suppress instabilities. Using the maximum voltage, the synchrotron tune at 5 GeV is of order 0.3. If we plan on exploiting this feature it is likely we will need to distribute the RF cavities around the ring. With 30 cavities we could have 3 sets of 10 or 6 sets of 5. It will be necessary to do the relevant particle tracking to estimate the impact of longitudinal chaos.

4.3.2 Crab Cavities

The crab cavities need to compensate a total crossing angle of θ = 0.015. The crab cavity voltage is

$$V_x = \frac{\theta E_T / q}{2k\sqrt{\beta^* \beta_k}\,\sin\Delta\psi_x}$$

Where the IP horizontal beta function is β^* = 2.2 m, at the crab cavities β_k = 2400 m and $\Delta\psi_x$ = 85° is the phase advance between the IP and the cavity. The total energy divided by the charge is E_T/q =250 GV. The wavenumber associated with the cavity frequency is k. The following figure illustrates the situation for a 112 MHz cavity.

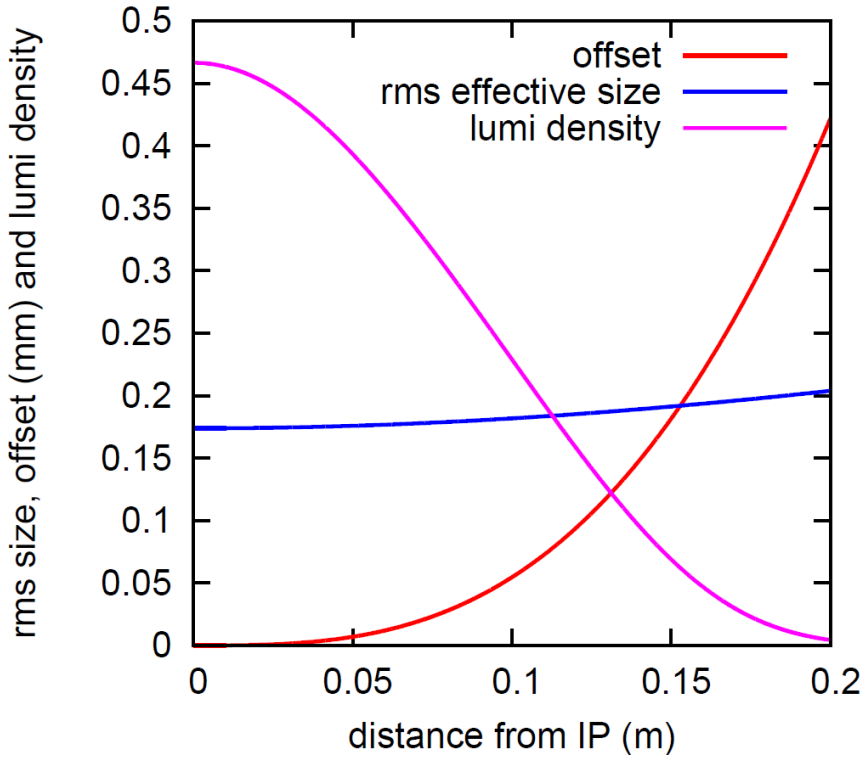

Figure 3-9: RMS effective size, offset and lumi-density as function of distance from Interaction Point.

In figure 3-9 the luminosity density for head on collisions is plotted. With the cavity this is decreased by the factor

$$L(s) = L_0(s)\exp\left(\frac{offset^2}{2\sigma_{eff}^2}\right)$$

Where σ_{eff} is the RMS effective size and the offset is the difference between the actual ion beam centroid and the ideal beam centroid. A single kicker frequency of 112 MHz restores 90% of the head on luminosity but there are significant offsets of particles near the head and tail of the bunch. Tracking simulations need to be done to see if there are dynamical issues.

Assuming the dynamical issues are OK the crab cavity needs a transverse voltage V_x = 11.2 MV. Taking a radius of r = 10 cm yields a maximum longitudinal voltage of $V_z = kr\ V_x$ = 2.6 MV. These voltages will occur on the right and left apertures and be of opposite sign for the two sides. It is probably necessary to make the device superconducting. The crab cavities proposed for the LHC operate at 400 MHz and supply 3 MV of transverse voltage. If we keep the magnitude of the electric and magnetic fields the same and increase all dimensions by a factor of 4 we can get a single 100 MHz cavity with a transverse voltage of 12 MV. While this estimate is clearly naïve it should serve as an existence proof for the actual cavities we will need to build.

4.4 Beam Physics

4.4.1 Electron Polarization

Achieving high polarization

The achievable beam polarization level in electron circular accelerators is defined mostly by two processes related to synchrotron radiation: Sokolov-Ternov self-polarization and depolarization caused by synchrotron radiation quantum emission. The self-polarization process leads to a slow build-up of electron polarization in the direction opposite to the vertical guiding field, up to a maximum level of 92.4% in an accelerator without spin rotators and with sufficiently weak spin resonances.

However, the presence of spin rotators, wigglers, as well as strong spin resonances reduces the achievable polarization level. An important quantity is also the self-polarization time, which has a strong dependence on the beam energy, scaling like E^{-5}. The self-polarization time for an eRHIC storage ring in the energy range of interest is shown in

Figure 3-10. The self-polarization time is long over practically all of energy range, except approaching 20 GeV where it drops to about 30 minutes. This demands a full energy polarized electron injector, so that the electron beam is injected into the storage ring with high polarization – 70% to 80%. One benefit of the long self-polarization time is that spin patterns containing bunches of opposite polarization orientation can be used.

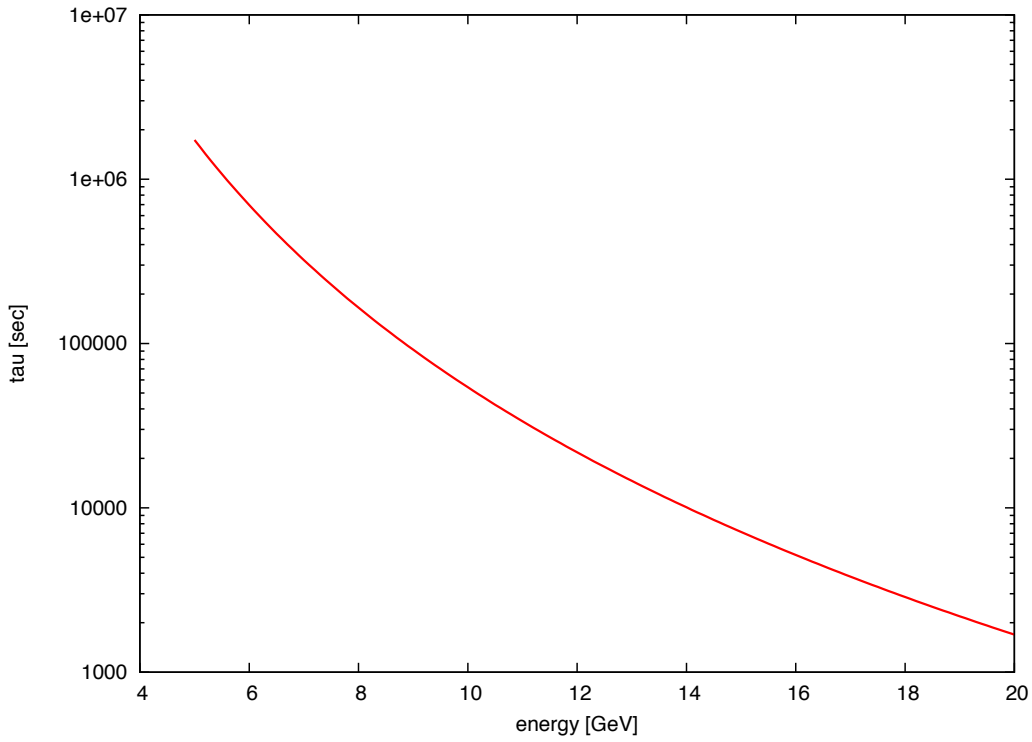

Figure 3-10: Sokolov-Ternov polarization time in the eRHIC electron storage ring as a function of energy.

The main challenge of spin dynamics in the storage ring is to preserve the high polarization level of the injected beam, at least at energies that are far from spin resonance conditions. The required timescale of polarization preservation is defined by the time interval between electron beam re-injections. Depolarizing effects are dominated by spin diffusion caused by the quantum nature of synchrotron radiation emission. In the presence of synchrotron radiation related spin diffusion the equilibrium polarization is described by the Derbenev-Kondratenko formula [4].The depolarizing time τ_{dpl} is defined by the diffusion rate of beam energy spread and the sensitivity of the stable spin solution n to the particle energy:

$$\frac{1}{\tau_{dpl}} = \frac{1}{2}\left\langle \left| \gamma \frac{\partial \boldsymbol{n}}{\partial \gamma} \right|^2 \frac{d\left(\delta\gamma/\gamma\right)^2}{dt} \right\rangle_\theta$$

where γ is the relativistic factor and the averaging inside angle brackets is done over accelerator azimuth θ and, in general, over the beam phase space.

The strength of depolarizing effects increases as E^7, thus making it more difficult to maintain high polarization in storage rings at higher energies. Nonetheless, Figure 3-11 shows that several accelerators operating above 10GeV have achieved high electron polarization level, exceeding 60% [5]. The accelerator technology used to achieve high polarization at high energies included highly efficient orbit correction, beam-based alignment of Beam Position Monitors relative to quadrupole field centers, and harmonic spin matching [6]. These tools are mitigate the effects of imperfection spin resonances and their synchrotron sidebands.

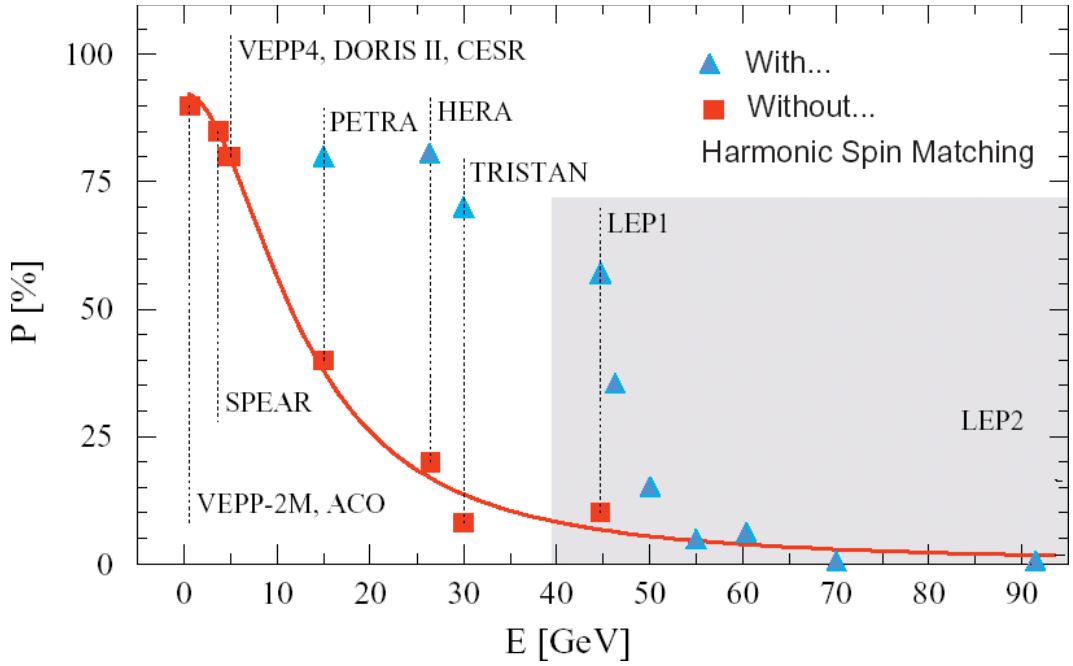

Figure 3-11: Electron polarization levels achieved in various circular electron storage rings [5].

In addition, the intrinsic resonances must be narrow enough to preserve high polarization, at least at energies far enough away from spin resonance conditions. Betatron coupling and unmatched spin rotator insertions can considerably widen the spin resonances, decreasing the achievable polarization. Thorough spin simulation studies have yet to be performed, to determine the tolerances on the closed orbit and betatron coupling control, and the required efficiency of spin matching and correction techniques. The storage ring uses damping wigglers to increase the damping decrement at lower energies, and to adjust the electron path length. Wiggler-enhanced synchrotron radiation increases the spin diffusion rate. Thus, careful attention must be paid to the possibility of enhanced depolarization at lower energies. Similarly, the effect of beam-beam interactions on polarization needs attention, since large electron beam tune spreads would effectively widen the intrinsic resonances.

Spin rotators

Spin rotators are needed to convert the vertical polarization of the electron beam in the arcs to a longitudinal polarization at the experimental detector. The state-of-the-art electron spin rotator that was used in the electron-proton collider HERA (DESY, Germany) [7] was 56 m long. It employed a sequence of interleaved vertical and horizontal dipole magnets to transform the vertical spin of 27 GeV electrons to the required orientation in the horizontal plane. The vertical orbit excursion inside the spin rotator was quite large – about 20 cm – thus requiring some of the rotator magnets to be shifted vertically from the plane of the HERA electron ring.

The eRHIC spin rotators must operate over a large energy range, from 5 GeV to 20 GeV. Since the orbit excursion in the dipole magnets scales inversely with the beam energy, a HERA-type rotator leads to 1m orbit excursions of 5 GeV electrons. Further, the synchrotron radiation power (per meter) produced by 20 GeV eRHIC electrons is considerably larger than the 27 GeV electrons in HERA, due to the much large electron current. Reducing the linear power load requires further increasing the rotator length and, correspondingly, the vertical orbit excursion. Therefore, the only practical solution is a spin rotator based on strong solenoid magnets. Solenoidal Siberian Snakes have been used in electron accelerators operating in the 0.5 GeV to 1 GeV range [8]. The integrated longitudinal field necessary to rotate the electron spin by 90 degrees, from the vertical to the horizontal, is

$$BL\ [Tm] = 5.240\ E\ [GeV]$$

A solenoid-based scheme for eRHIC using two rotators is shown in Figure 3-12. The first rotator (sol1) is used for operations in the 5 GeV to 10 GeV energy range. A second rotator (sol2) is also excited in the 10 GeV to 20 GeV energy range. The total spin rotation produced at any energy is 90 degrees. Each spin rotator contains two solenoids, and at least 5 skew quadrupoles to compensate for the betatron coupling and the vertical dispersion. lists the main parameters of the rotators. The maximum field integrals of 53 Tm and 105 Tm can be realized by using superconducting magnets with fields in the 7 T to 10 T range. High-temperature superconducting technology might be used to produce even higher fields.

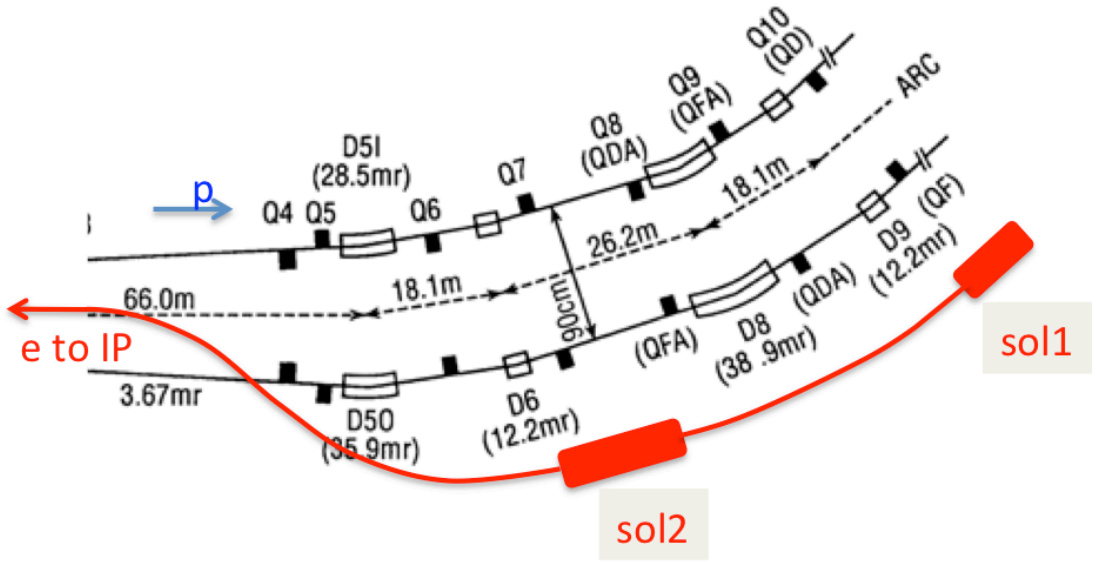

Figure 3-12: Layout of the electron spin rotators.

Perfect longitudinal polarization at the interaction point is only achieved at 7.5 GeV and 15 GeV, in the suggested scheme. Figure 3-13 shows the slight deviations of the polarization orientation that occur at other energies, with a worst-case longitudinal spin projection reduction of 13%.

Table 3-7: Spin rotator parameters.

Parameter	sol1	sol2
Energy range [GeV]	5 – 10	10 – 20
Field integral range [Tm]	26 – 53	52 – 105
Length (at 7 T)	7.6	15.0
Orbit angle from the IP [mrad]	92	46
Location in the RHIC tunnel	D9 – D10	D6 – Q8

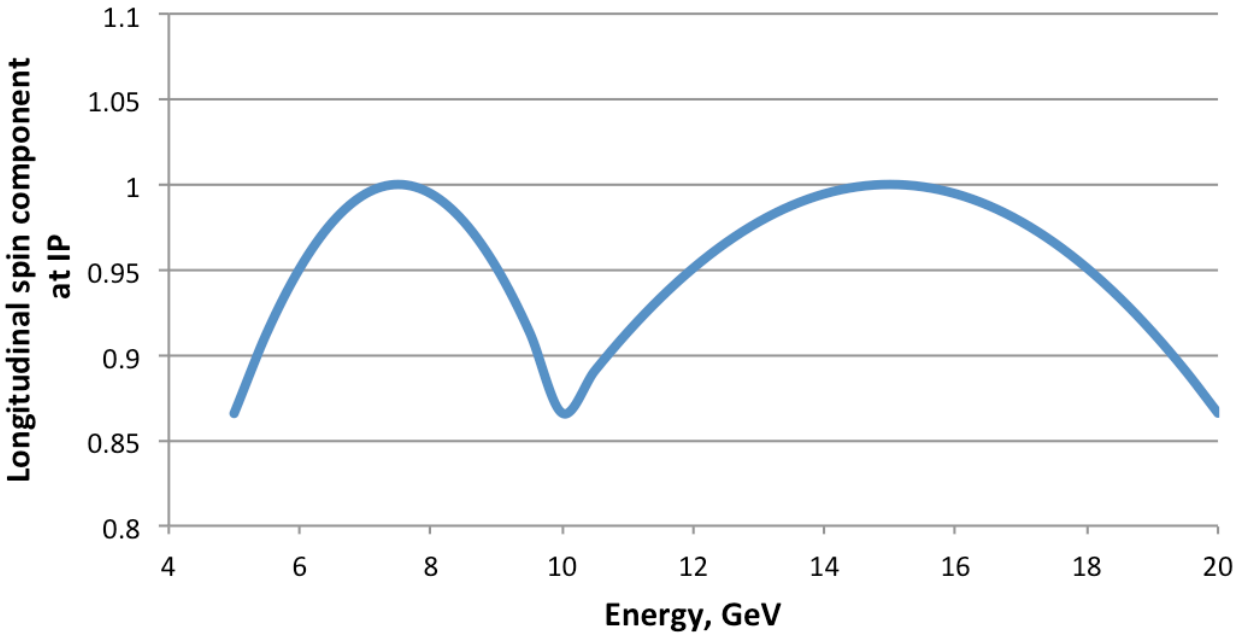

Figure 3-13: Deviation of the polarization orientation as a function of energy.

Spin matching conditions on the beam optics have to be established and satisfied, in order to minimize the depolarization effects caused by synchrotron radiation induced diffusion. The future evaluation of depolarizing effects and spin matching must include the effect of the detector solenoid, with an integrated strength in the 4 Tm to 5 Tm range. In general, spin matching conditions with solenoid spin rotators will be energy dependent. The machine optics must satisfy them at all electron energies in the range from 5 GeV to 20 GeV.

Spin flipping

To realize arbitrary spin patterns in the electron beam, electron bunches with spins up and down need to be injected into the eRHIC electron storage ring. In bunches with spin "down" single electrons will flip their spin to the "up" direction, with the Sokolov-Ternov time constant shown in Figure 3-10. This will effectively depolarize those bunches. Entire bunches (or bunch trains) need to be replaced on a regular basis. This suggests that electron injection will look exactly the same as proton injection – on-orbit and on-energy. In this scenario there should not be any significantly enhanced background in the detectors due to electron injection.

With the shortest Sokolov-Ternov polarization time of about 1600 seconds at an energy of 20 GeV, continuously replacing single bunches at 1 Hz would take 6 minutes for a 360-bunch fill. In reality it is sufficient to only replace those bunches with spin "down", which would only take 3

minutes. This is sufficiently short compared to the Sokolov-Ternov polarization time, so that depolarization of those bunches is small even at 20 GeV.
Electron bunch intensity accumulation is necessary in the injector system if full-intensity bunches are to be injected into the storage ring, since the required intensity is about a factor of five larger than the intensity of the ERL Gatling gun design. This accumulation could be performed either in a rapid cycling synchrotron, or in a separate accumulator/damping ring, if a linac injector scheme is chosen. Such a dedicated accumulator/damping ring might be installed in the existing AGS tunnel.

4.4.2 Electron Cooling

Table 3-8 lists beam parameters and calculated IBS growth times for nominal design parameters of protons at 50, 160 and 250 GeV for the Ring-Ring approach.

Table 3-8: Nominal parameters for eRHIC protons beam for the Ring-Ring approach.

	Proton		
Energy [GeV/n]	50	160	250
Bunch frequency [MHz]	28	28	28
Bunch intensity [10^{11}]	3	3	3
RMS normalized emittance [10^{-6} m]	2.5	2.5	2.5
Longitudinal bunch area [eVs]	0.32	0.66	1.6
RF frequency [MHz]	197	197	197
RF voltage [MV]	0.48	1.8	3
RMS momentum spread [10^{-4}]	5.2	5.2	5.2
RMS bunch length [cm]	19.6	20	19.5
IBS growth time for longitudinal emittance [min]	25	131	250
IBS time for horizontal and vertical emittance [min], fully coupled	198	320	407

For nominal parameters with protons at 250 and 160 GeV beam growth due to the Intra Beam Scattering (IBS) is not significant so that cooling of protons at these energies is not required.
For the lowest energy of protons of 50 GeV cooling would be needed to obtain small longitudinal emittance first, as well as to compensate IBS for such beam parameters. Required cooling time could be obtained with high-energy magnetized electron cooler or electron cooler without magnetization.

For baseline parameters with protons at 250 GeV beam growth due to Intra Beam Scattering is not significant. Presently, the 95 % longitudinal emittance of protons at RHIC injection is about 1.6 eV-s. For the top energy with 3 MV on 197 MHz RF this would correspond to an RMS bunch length of 0.2 m and RMS momentum spread of 5×10^{-4}. The corresponding IBS growth times of the horizontal and vertical beam emittances (with full coupling between horizontal and vertical planes) are 407 minutes and the IBS growth time of the longitudinal emittance is 250 minutes.

For protons at 160 GeV to get longitudinal RMS bunch length of 0.2 m it is assumed that one should be able to get the longitudinal emittance of 1.0 eV-s from the RHIC injectors or by pre-cooling at RHIC injection energy. The resulting IBS growth times of the horizontal and vertical beam emittances are 320 minutes and the IBS growth time of the longitudinal emittance is 130 minutes.

For protons at 50 GeV to get longitudinal RMS bunch length of 0.2 m one would need to obtain the longitudinal emittance of protons significantly smaller than presently achieved for high-intensity protons at RHIC injection energy. For IBS calculation at 50 GeV it was assumed that longitudinal emitance of 0.3 eV-s can be obtained by pre-cooling at RHIC injection energy or by

cooling directly at 50 GeV. The resulting IBS growth times of the horizontal and vertical beam emittances (fully coupled) are 198 minutes and the IBS growth time of the longitudinal emittance is 25 minutes.

Electron cooling technique uses co-propagating electron beam in a localized portion of a circular ion accelerator to obtain high-intensity ion beams with low momentum spread. Its underline physical mechanism is the dynamical friction experienced by individual ions moving in the co-propagating electron distribution.

Existing electron cooling systems are based on an electron beam generated with electrostatic DC electron gun, immersed in a longitudinal magnetic field. For cooling of 50-250 GeV protons one needs 27-136 MeV electrons, respectively, which makes the use of electrostatic acceleration unviable. RF acceleration of a bunched electron beam results in an electron transverse momentum spread significantly larger than in existing electrostatic coolers.

Electron cooling times grow rapidly with beam energy making direct cooling of protons at high energies not effective. This suggests a staged cooling for high-energy protons, where an initial cooling is first done at low energy close to the injection. At low proton energies in the range 25-50 GeV, cooling becomes more rapid and can be used to control or pre-cool transverse and longitudinal beam emittances to required values.

When an RMS velocity spread within electron beam is comparable or smaller than the spread within the ion beam and, and there is no requirement of getting ultra-cold ion state, the cooling can be done without the help of the strong external magnetic field. Such type of cooling is referred to as the "non-magnetized cooling"; although a weak external field can be still employed, for example, to ensure focusing and alignment of electron and ion beams. Electron cooling using the non-magnetized electron beam can significantly simplify the cooler design. However, for non-magnetized cooling one needs to have the transverse RMS velocity spread of the electron beam to be comparable to the one of the ions. For eRHIC ring-ring baseline parameters the emittance of hadron beam is about 2.5 μm. As a result, for the non-magnetized cooling approach to be effective electron bunch emittance should not be much larger than 2.5 μm. Achieving required electron bunches with such transverse emittance for cooling at 50 GeV appears to be feasibly making non-magnetized cooling approach attractive. Needed electron cooling parameters are summarized in Table 3-9. If necessary, requirement on electron bunch charge can be further reduced by pre-cooling first at even lower energy.

Table 3-9: Electron cooler parameters for non-magnetized cooling approach.

	Electron
Relativistic factor	53
Length of cooling section [m]	120
Bunch charge [nC]	6
RMS normalized emittance [10^{-6} m]	2.5
RMS bunch length [cm]	20
RMS momentum spread [10^{-4}]	5
Cooling time longitudinal [min]	23
Cooling time transverse [min]	95

The presence of a strong longitudinal magnetic field changes the collision kinetics significantly. The magnetic field limits transverse motion of the electrons. In the limit of a very strong magnetic field, the transverse degree of freedom does not take part in the energy exchange, because

collisions are adiabatically slow relative to the Larmor oscillations. As a result, the efficiency of electron cooling is determined mainly by the longitudinal velocity spread of the electrons. Such type of cooling is typically referred to as a "magnetized cooling". Magnetized cooling was found extremely useful technique in obtaining high-brightness hadron beams at low energies.

The use of magnetized cooling does not have strict requirement on transverse emittance of electron bunches. However, the disadvantage of magnetized cooling is that it requires significantly higher than non-magnetized cooling electron bunch charge because the Coulomb logarithm for slow collisions, which determine efficiency of magnetized cooling, is much relatively small. Another disadvantages of magnetized cooling are more technologically challenging electron beam transport as well as cooling section solenoids. Such complication appears to be unnecessary for parameters of protons in Table 3-8 at 50 GeV since achieving emittance of few microns for electron charge of 6nC, as needed with the non-magnetized cooling approach summarized in Table 3-9, appears to be feasible.

4.4.3 Crab Crossing

The 15 mrad full crossing angle between the electron and ion beam at the interaction point requires crab crossing to restore the luminosity. With the crab cavities installed at a betatron phase of $\frac{\pi}{2} + k\pi$ from the interaction point (IP) at a location with β_{crab}, the required crab cavity voltage is computed as

$$V_{crab} = \frac{\theta_{crab} E[GeV]}{2\pi\, f_{crab} \sqrt{\beta_{crab}\beta_{IP}}}$$

Here, θ_{crab} is half the total beam crossing angle, E the beam energy in GeV, f_{crab} the crab cavity RF frequency, and β_{IP} the β-function at the interaction point.

Using θ_{crab} = 7.5 mrad, β_{crab}= 2400 m, and f_{crab} = 112 MHz, the required crab cavity voltage for 250 GeV protons is therefore 11.2 MV. This restores 91% of the head on luminosity; additional gains require higher harmonic crab cavities to linearize the kick. Tracking simulations are currently under way to determine whether such higher harmonic crab cavities are also required in terms of beam-beam dynamics.

In the interaction region design presented in this report the crab cavities are located at a less-than-perfect betatron phase advance of 86^o from the IP. This results in an additional, undesirable orbit angle for the head and the tail of the ion bunches at the IP. This angle is described by the M_{22} element of the transfer matrix from the crab cavity to the IP:

$$M_{22} = \sqrt{\frac{\beta_{crab}}{\beta_{IP}}}\, cos\varphi_{crab} \approx 2.$$

To correct this angle error, a second set of crab cavities at a betatron phase advance of $\varphi_{corr} = k{\times}180^o$ from the IP is needed. The corrective effect of this cavity is described my its matrix element:

$$m_{22} = \sqrt{\frac{\beta_{corr}}{\beta_{IP}}} * cos\varphi_{corr} = \pm\sqrt{\frac{\beta_{corr}}{\beta_{IP}}}.$$

By choosing a location such that $m_{22} > M_{22}$, we ensure that the required voltage on this second set of crab cavities is does not exceed that of the main crab cavity set. This condition is fulfilled if $\beta_{corr} >$ 10 m, which is the case almost everywhere in the electron ring except for special locations such as the IP and its immediate vicinity.

4.4.4 Collective effects

Instabilities in the electron ring have been studied using a modified version of TRANFT, which was used during the design of NSLS-II and evolved into the stochastic cooling simulation code. Simulations were done for electron energies of 5 GeV, 10 GeV and 20 GeV. The momentum compaction factors, partition numbers and other parameters were taken from Table 3-5. Only single bunch instabilities were considered. Given the preliminary stage of design the longitudinal and transverse impedances were modeled as resonators with quality factor 1 and resonant frequency 10 GHz. The longitudinal impedance was adjusted to make $Im\left(\frac{Z}{n}\right) = 1\ \Omega$ at low frequency and the transverse impedance at low frequency was $Z_x = Z_y = 1.4$ MΩ/m. The simulations were done with zero synchronous phase and 40 MV of RF cavity voltage at $h = 18\times360$, 508 MHz. The effect of synchronous phase should be negligible given the short electron bunches.

For 10 GeV and 20 GeV the bunch was stable for 10^{12} electrons per bunch, a factor of 3 or more above design intensity. For 5 GeV the bunches were stable with $3\text{x}10^{11}$ electrons per bunch but unstable with 10^{12}. Additional simulations showed this was due to the very small value of $J_x = 0.1$, leading to a radiation damping time of 120 ms. When the transverse radiation damping time was reduced the 12 ms the 5 GeV bunch was stable with 10^{12} electrons.

Bibliography

[1] S. Y. Lee, Accelerator Physics, 1999
[2] The MADX Program, 2013, http://mad.home.cern.ch/mad
[3] PEP-II Conceptual Design Report, SLAC-418, 1993
[4] Ya.S. Derbenev and A.M. Kondratenko, Sov. Phys. IJETP 35 2306A (1972)
[5] S.R. Mane, Yu. M. Shatunov and K. Yokoya, Report on Progress in Physics 68 1997 (2005).
[6] R. Assmann et al., Proceedings of EPAC, London, p.932 (1994).
[7] D.P. Barber, et al., Phys. Lett. 3434B 436 (1995).
[8] T. Zwart, et al., Proceedings of PAC, Chicago, p.3597 (2001).